arXiv:astro-ph/9611056v1 7 Nov 1996

Coalescing neutron stars – gravitational waves from polytropic models

M. Ruffert[*], M. Rampp[**], and H.-Th. Janka[***]

MPI für Astrophysik, Postfach 1523, D-85740 Garching, Germany

February 1, 2008

Abstract. The dynamics, time evolution of the mass distribution, and gravitational wave signature of coalescing neutron stars described by polytropes are compared with three simulations published previously: (a) "Run 2" of Zhuge et al. (1994), (b) "Model III" of Shibata et al. (1992), and (c) "Model A64" of Ruffert et al. (1996). We aim at studying the differences due to the use of different numerical methods, different implementations of the gravitational wave backreaction, and different equations of state. We integrate the three-dimensional Newtonian equations of hydrodynamics by the Riemann-solver based "Piecewise Parabolic Method" on an equidistant Cartesian grid.

Comparison (a) confronts the results of our grid-based PPM scheme with those from an SPH code. We find that due to the lower numerical viscosity of the PPM code, the post-merging oscillations and pulsations can be followed for a longer time and lead to larger secondary and tertiary maxima of the gravitational wave luminosity and to a stronger peak of the gravitational wave spectrum at a frequency of about $f \approx 1.8$ KHz when compared to the results of Zhuge et al. (1994). In case (b) two grid based codes with the same backreaction formalism but differing hydrodynamic integrators and slightly different initial conditions are compared. Instead of rotationally deformed initial neutron stars we use spherically shaped stars. Satisfactory agreement of the amplitude of the gravitational wave luminosity is established, although due to the different initial conditions a small time delay develops in the onset of the dynamical instability setting in when the two stars come very close. In (c) we find that using a polytropic equation of state instead of the high-density equation of state of Lattimer & Swesty (1991) employed by Ruffert et al. (1996) does not change the overall dynamical evolution of the merger and yields agreement of the gravitational wave signature to within 20% accuracy. Whereas the polytropic law describes the dynamical behaviour of the bulk of the matter at and above nuclear density sufficiently well, we, however, find clear differences of the structure and evolution of the outer layers of the neutron stars where the stiffness of the equation of state is largely overestimated. This has important implications for questions like mass loss and disk formation during the merging of binary neutron stars.

Key words: Hydrodynamics – Binaries: close – Stars: neutron – Gravitation: waves

Send offprint requests to: M. Ruffert

[*] e-mail: mruffert@mpa-garching.mpg.de

[**] e-mail: mrampp@mpa-garching.mpg.de

[***] e-mail: thj@mpa-garching.mpg.de

1. Introduction

Coalescing neutron stars are interesting and powerful sources of gravitational waves. These mergers — together with black holes, rapidly rotating neutron stars, and supernovae — are among the most promising candidates (Thorne 1992) to be detected with the large gravitational wave experiments that will soon be operational or are currently planned, LIGO (Abramovici et al. 1992), VIRGO (Bradaschia et al. 1991), GEO600 (Danzmann et al. 1995a), and the space-based LISA (Danzmann et al. 1995b). The detectability does not only depend on the strength of the emission, but also on the frequency of the gravitational waves relative to the resonance frequencies of the detectors (Finn & Chernoff 1993; Finn 1994). Only an a priori knowledge of the structure of typical gravitational wave signals allows the extraction of faint signals from a very noisy background. Theoretically predicted wave templates have to be produced by numerical simulations. Additionally to being sources for gravitational waves, coalescing neutron stars (and its relative, the merger of a neutron star with a black hole) remain the favorite cosmological model for gamma-ray bursters (Dermer & Weiler 1995) because the sources are known to exist, the right amount of energy is involved, and the expected merger rates are in agreement with the required gamma-ray burst rates.

The search for gravitational waves thus calls for models of coalescing neutron stars that are numerically highly resolved and as realistic as possible. Several groups have attempted such investigations and have published results. In a series of papers starting with Oohara & Nakamura (1989) a Japanese group used variations of a grid-based code to find the gravitational wave luminosity for different conditions, e.g. different masses, initial separation or spins of the neutron stars (Shibata et al. 1993, and references therein). Zhuge et al. (1994) concentrated on the energy spectrum that gives the energy emitted in gravitational waves at different frequencies. They discussed the information about the dynamics of the coalescence that may be extracted from a measured spectrum. Focussing on dynamics and stability, Rasio & Shapiro (1994) found that *triaxial* configurations are formed by the merging of neutron stars with a sufficiently stiff polytropic equation of state. Non-axisymmetric structures occur for adiabatic exponents of 3 or higher (polytropic index 0.5 or below). In this case the peak amplitude of the gravitational wave emission is substantially larger and the emission proceeds for a longer time after the coalescence.

Our treatment of the gravitational wave backreaction is identical to what has been used by Shibata et al. (1992). We consider this procedure to be more accurate than the point-mass quadrupole approximation used by Davies et al. (1994) and Zhuge et al. (1994). Their approximation was used when the neutron stars were still separated and subsequently switched off when the merging took place. Although Rasio & Shapiro (1994) investigated the stability of the neutron star binary orbit in detail, they did not take into account the gravitational radiation reaction at all.

The three investigations done by Davies et al. (1994), Zhuge et al. (1994) and Rasio & Shapiro (1994) all used SPH codes, whereas our simulations, as well as the ones by Shibata et al. (1992), were performed with explicit, Eulerian, finite-difference grid-based schemes. The algorithm we use is based on the PPM-scheme of Colella & Woodward (1984) which is a higher-order Godunov-type method in that it locally solves Riemann problems. It is thus superior to a particle-based method like SPH in the handling of shocks and also has a rather small numerical viscosity compared to other Eulerian algorithms and SPH.

We chose to compare our numerical scheme with the following three calculations. (1) "Run 2" of Zhuge et al. (1994) was chosen since in this model the neutron stars have masses and radii similar to those in Ruffert et al. (1996) (although the equations of state were different). Additionally, the published detailed spectral analysis of the gravitational wave emission is well suited for comparisons. (2) "Model III" of Shibata et al. (1992) was selected, because their numerical scheme is grid-based and the algorithm to treat the gravitational wave backreaction is similar to ours. Therefore differences of the results are associated with differing hydrodynamical integrators and

numerical resolution. In both cases (1) and (2), polytopic equations of state were used which we also applied in our comparative calculations. (3) "Model A64" of Ruffert et al. (1996) served for comparison in order to investigate the differences caused by the use of a polytropic equation of state instead of the more realistic equation of state of Lattimer & Swesty (1991) which allowed Ruffert et al. (1996) also to include the effects due to neutrino emission.

We did not select a model computed by Davies et al. (1994) because although their computations were done with a polytropic equation of state, they did not give information about the gravitational wave emission, since their formula was too crude. Rasio & Shapiro (1994), on the other hand, were very careful in constructing equilibrium models and in investigating the stability of these models as well as the gravitational wave forms and luminosity. Nevertheless, we preferred for our present investigations a comparison with a run of Zhuge et al. (1994), because (a) Rasio & Shapiro (1994) did not include any backreaction of the gravitational waves, and (b) the spectra presented by Zhuge et al. (1994) were better suited for comparisons.

Section 2 gives a brief description of the numerical methods, introduces the set of computed models and details the initial conditions that our simulations are started from. The results of our computations and the comparison with previous published models are presented in the three Sects. 3, 4, and 5, separately. A summary follows in Sect. 6.

2. Computational procedure and initial conditions

The numerical procedures implemented to simulate our models of coalescing neutron stars were described in detail in a first paper (Ruffert et al. 1996). In the following, we shall specify only the differences of the treatment of the presented polytropic models compared to what has been described in Ruffert et al. (1996).

2.1. Hydrodynamics and equation of state

The neutron stars are evolved hydrodynamically via the Piecewise Parabolic Method (PPM) developed by Colella and Woodward (1984). The code is basically Newtonian, but contains the terms necessary to describe gravitational waves and their backreaction on the hydrodynamical flow (Blanchet, Damour & Schäfer 1990) via energy and angular momentum loss. The volume integral over the local emission and backreaction terms yields the total gravitational wave luminosity. All spatial derivatives necessary to compute the gravitational wave terms are implemented as standard centered differences on the grid.

The Poisson equations in integral form, necessary for the calculation of the gravitational potential as well as for the wave backreaction, are interpreted as convolution and calculated by fast Fourier transform routines: non-periodic grid boundaries are enforced by zero-padding (e.g. Press

Table 1. Parameters of the three Models ZCM, SNO, and RJS. R is the initial radius of the two identical neutron stars, ρ_0 their initial central density, a_0 the initial center-to-center separation of the stars, M the mass of the neutron stars, K the polytropic constant, Γ the adiabatic exponent, L the grid size, N the number of zones per dimension, t_f the total time interval of the run, $\mathcal{E}$ the total energy emitted in gravitational waves within time t_f, $\widehat{\mathcal{L}}$ is the maximum gravitational-wave luminosity, and $r\widehat{h}$ is the maximum amplitude of the gravitational waveforms observed from a distance r

Model	R km	ρ_0 $10^{14}\frac{\text{g}}{\text{cm}^3}$	a_0 km	M $M_\odot$	K	Γ	L km	N	t_f ms	$\widehat{\mathcal{L}}$ 10^{55}erg	$r\widehat{h}$ 10^4cm	$\mathcal{E}$ $10^{52}\frac{\text{erg}}{\text{s}}$	notes reference, model name
ZCM	15	6.4	45	1.4	$9.7 \cdot 10^4$	2.0	88	64	8.7	2.0	1.9	0.88	Zhuge et al. (1994), Run 2
SNO	9	29.6	27	1.4	$3.5 \cdot 10^4$	2.0	52	128	2.0	8.3	3.2	13.6	Shibata et al. (1992), Model III
RJS	15	5.7	42	1.63	2.438	2.319	82	64	4.6	2.8	2.6	2.07	Ruffert et al. (1996), Model A64

et al. 1992; Eastwood & Brownrigg 1979). The accelerations that follow from the potential are added as source terms into the PPM algorithm. For models ZCM and RJS the number of cubic grid zones in the orbital plane is 64 by 64, while perpendicular to the orbital plane 16 zones were used with the same zone size in all three dimensions. We use double the amount of zones (128) in every spatial direction for model SNO in order to have a similar number of zones (121) as Shibata et al. (1992). We take advantage of the symmetry about the orbital plane to actually calculate only one side of the plane.

A polytropic equation of state,

$$P = K\rho^\Gamma \quad , \tag{1}$$

is used which relates the density ρ to the pressure P via two parameters, the polytropic constant K and the adiabatic exponent $\Gamma = 1 + \frac{1}{n}$, with n being the polytropic index. This equation with K and Γ chosen to be the same in the whole star was employed to construct the initial model of the neutron star. Since the PPM code is written in conservative form (not taking into account source terms like gravity), the primary variables are the density, the momentum, and the total energy. One therefore has the choice of using either Eq. 1 to calculate the pressure from the density or the relation

$$P = (\Gamma - 1)e \tag{2}$$

to deduce the pressure from the internal energy density e. Analytically these formulations are equivalent, but numerical errors may destroy this equivalence. When shocks or viscous shear dissipation occurs in the hydrodynamic calculations, the use of Eq. 2 is preferable because due to the dissipative processes the parameter K of Eq. 1 is not a strict constant in space and time during the simulations. If one postulates analytical equivalence of the pressure in Eq. 2 with the polytropic equation of state, Eq. 1, the generation of thermal energy in shocks manifests itself in a variation of K. Eq. 1 was used to construct the initial model and Eq. 2 to compute the hydrodynamic evolution. Due to these simple equations of state, effects of neutrino

emission, absorption or annihilation were not included in the present simulations.

2.2. Initial setup

Our initial setup involves placing two identical spherical neutron stars at some distance from each other and giving them an initial velocity. We prescribe the initial orbital velocities of the coalescing neutron stars according to the motions of point masses, as computed from the quadrupole formula. The tangential components of the velocities of the neutron star centers correspond to Kepler velocities on circular orbits, while the radial velocity components reflect the emission of gravitational waves leading to the inspiral of the orbiting bodies (for details, see Ruffert et al. 1996). A spin of the neutron stars around their respective centers is *not* added. Thus the initial state of the neutron star binary is defined by the following parameters: (a) center-to-center distance between the neutron stars and (b) three out of the following five quantities: mass, radius, and central density of the neutron star, and polytropic constant K, and adiabatic exponent Γ of the equation of state.

The initial distance at which the neutron stars are placed at the beginning of our simulations is a compromise between physical accuracy and computational resources. On the one hand we would like to start with the neutron stars at a large distance in order to correctly simulate the tidal deformation they experience during inspiral. However, the time to coalescence, which is proportional to the fourth power of the distance, increases by a huge amount if the distance between the neutron stars is only slightly increased. On the other hand, tidal deformation studies (e.g. Lai et al. 1994; Reisenegger & Goldreich 1994) show that tidal deformations for extended objects are only around 20% (for the principal axis) and normal mode excitation of at most a few percent of the neutron star radius at a distance of about 2.8 radii.

For numerical reasons it is not possible to do the simulations with arbitrary low density in the neutron star's environment. So the density of the matter in the surroundings of the neutron stars is set to 10^9 g/cm^3. To avoid
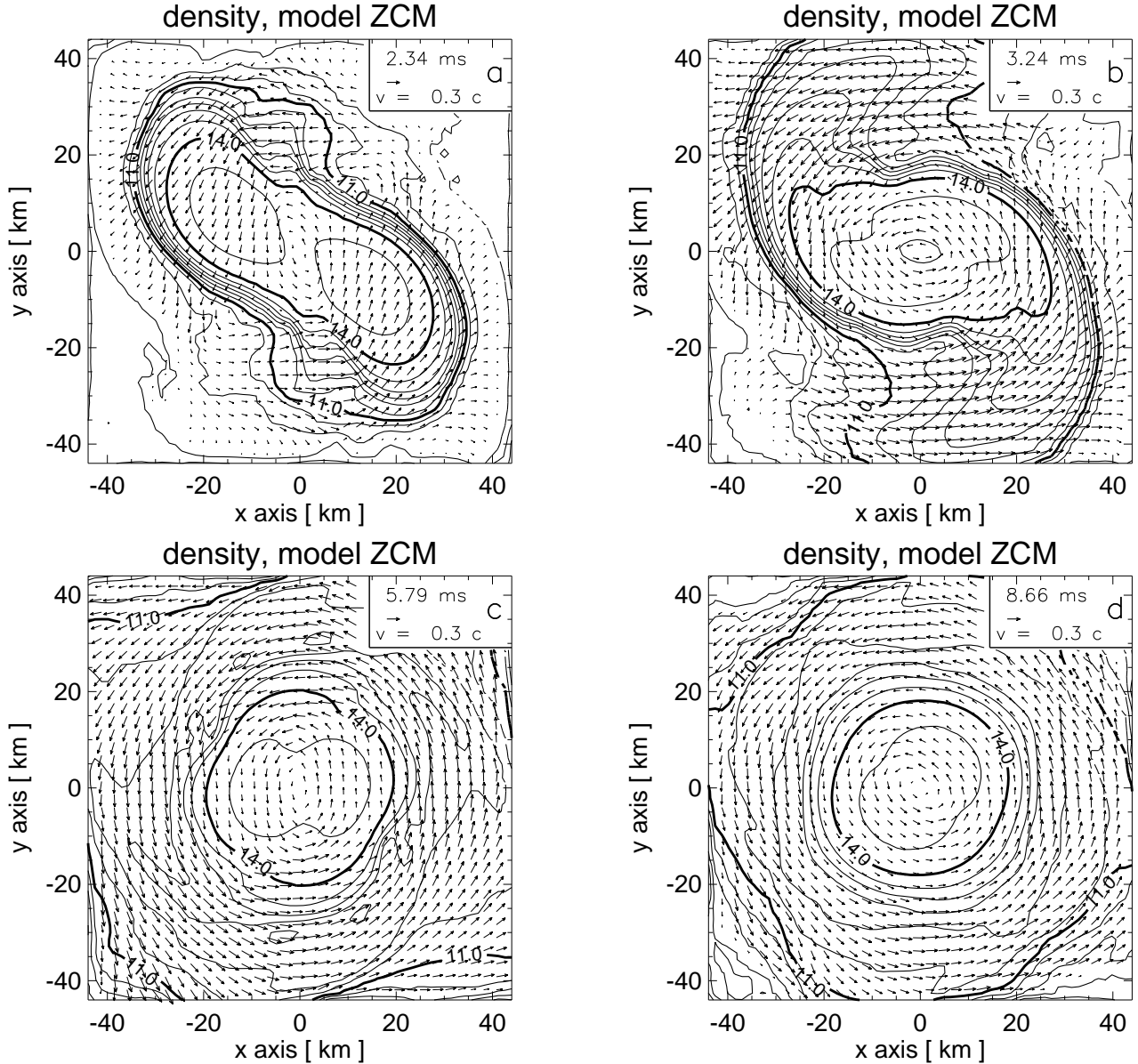
Fig. 1. Cuts in the orbital plane of Model ZCM at four instants in time showing the density contours together with the velocity field. The density contours are logarithmically spaced with intervals of 0.5 dex. The density is measured in units of g/cm^3. The bold contours are labeled with their respective values. The legend at the top right corner of each panel gives the scale of the velocity vectors and the time elapsed since the beginning of the simulation

this low-density matter being accelerated and falling onto the neutron stars, the velocities and kinetic energy are reduced to zero in zones in which the density is less than about $3 \cdot 10^9$ g/cm^3. With a numerical grid of roughly 1 km spatial resolution one cannot accurately represent the density decline near the surface of the neutron stars. We artificially soften the edge by imposing a maximal density change of 2 orders of magnitude from zone to zone. The thickness of the surface layer thus results to about 3 grid zones. To avoid short numerical time steps, we changed the constant K of the equation of state in the 3 surface zones such that the sound speed was constant within this broad-

ened surface layer. The same manipulation was applied for the surrounding gas at densities of about 10^9 g/cm^3.

We simulate three models with polytropic equations of state, the parameters of which are listed in Table 1. The initial conditions of each model are discussed in the respective section of the corresponding model. The calculations were performed on a Cray J90 8/512, needed about 3.2 MWords of main memory and approximately 25 CPU-hours for models ZCM and RJS, and 27 MWords and 140 CPU-hours for model SNO.

3. Results of Model ZCM

3.1. Initial conditions

We chose Run 2 of Zhuge et al. (1994), because the mass and radius of the neutron stars are closest to those of the stars which we have simulated in Ruffert et al. (1996). For Run 2, moreover, Zhuge et al. (1994) show the gravitational wave forms, the gravitational wave luminosity, and the energy spectrum. This case yields a direct comparison between the SPH computations with *ad hoc* gravitational backreaction done by Zhuge et al. (1994) and our Eulerian calculation of Model ZCM where backreaction is included.

Model ZCM has the same neutron star mass and radius as well as an adiabatic exponent of $\Gamma = 2$ as used by Zhuge et al. (1994) for their Run 2. In order to save CPU time we place the neutron stars at an initial distance of 45 km and *not* at the 60 km chosen by Zhuge et al. (1994). They were able to follow the inspiral from such a large distance because their SPH simulation was done with a comparatively small number of particles ($N = 1024$) which is computationally much cheaper than our grid-based simulations. Unfortunately, they do not show a plot of the neutron star separation as a function of time for Run 2. Without this relation the connection between the temporal evolution of their model and ours is not determined precisely. Thus we link our time to theirs by matching both calculations at the position of the first maximum of the gravitational wave luminosity (see Fig. 3) independent of how long it takes to spiral in from the initial separation of 60 km (used by Zhuge et al. 1994) to our initial separation of 45 km.

However, the information given by Zhuge et al. (1994) for their Run 1 can be used to interpret their Run 2. From their Fig. 10 one can infer at which time the separation of their neutron stars is $3R$, and then inspect their Fig. 1a to get an impression of the tidal deformations at that time: tidal bulges are visible but not dominant, in agreement with the analytical estimate of 20% deformation of the principal axis at a distance of $2.8R$ (see Sect. 2.2). We did not include these bulges in our initial setup of the neutron stars.

3.2. Dynamical evolution

Snapshots of the density distribution in the orbital plane together with the velocity field are shown for four times in Fig. 1. These plots give an impression of how the merging process proceeds. Within less than one orbital period the merging is well in progress (Fig. 1a). The typical transient spiral-arm pattern develops (Fig. 1b) due to tidal and centrifugal forces. One notices that for a fairly long time (for over 2 ms after $t = 4$ ms; e.g. Fig. 1c) the merged object has sort of a "double core" structure, visible by the dumb-bell shaped central contours. The quadrupolar deformation seems to be less pronounced in the model of Zhuge et al. (1994). It is damped only slowly and indica-
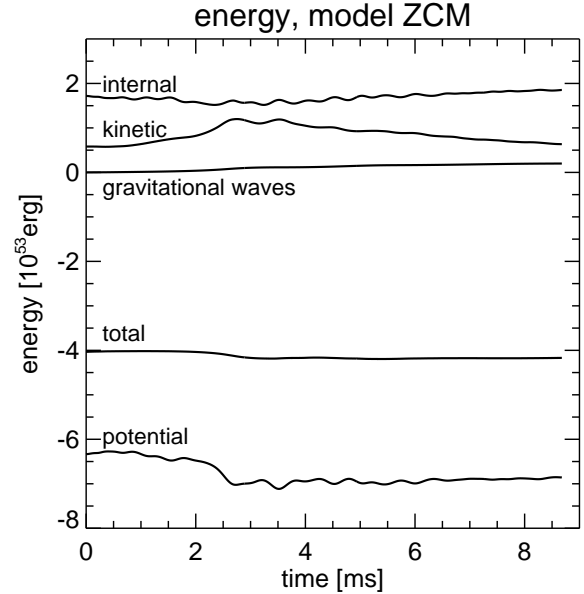

Fig. 2. Kinetic energy, internal energy, gravitational potential energy, and emitted gravitational wave energy as functions of time for Model ZCM. The total energy contains all individual energies
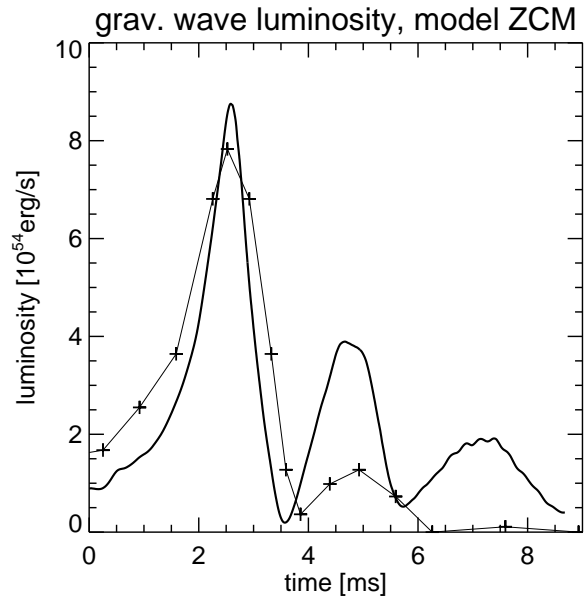

Fig. 3. The gravitational wave luminosity as a function of time for Model ZCM (solid line). The crosses represent the values of the gravitational wave luminosity taken from Fig. 16a in Zhuge et al. (1994) for their Run 2; they are connected by straight lines
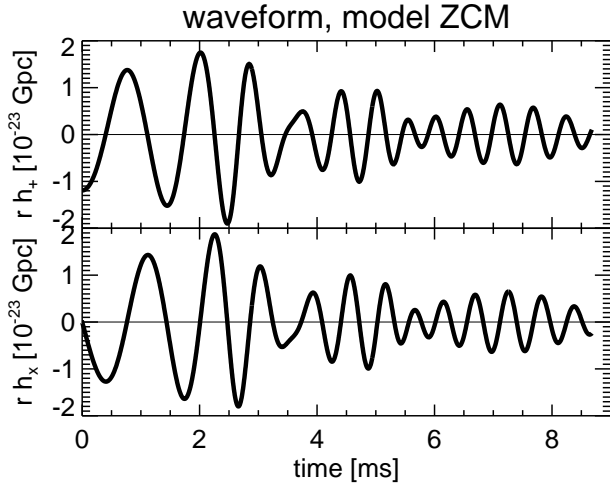
Fig. 4. The gravitational wave forms, h_+ and $h_\times$, for Model ZCM

tions of it are still present when we stop our simulation at $t = 8.7$ ms (Fig. 1d).

The temporal evolution of different energies is shown in Fig. 2. One notices that the coalescence is very smooth and that the potential energy decreases only by about 15%. The internal energy first decreases a bit due to tidal stretching, then increases again because some kinetic energy is dissipated into thermal energy, indicating the presence of shocks and friction. During the spiral-in and merging the maximum density decreases monotonically from roughly $6 \cdot 10^{14}$ g/cm^3 to $5 \cdot 10^{14}$ g/cm^3, because of tidal stretching before coalescence and internal "heating" due to shear effects which dissipate kinetic energy during coalescence.[1] The total energy is conserved to 2% compared to the maximum potential energy.

3.3. Gravitational wave forms and luminosity

The temporal structure of the gravitational wave luminosity is shown in Fig. 3 (the time integral of which can be seen in Fig. 2). The luminosity during the main merging event is of similar size in our Model ZCM and in Run 2 of Zhuge et al. (1994). Nevertheless, significant differences are visible: the maximum at $t \approx 2.5$ ms in our model is 10% higher and the width of the main peak about 40% narrower. Note that due to the difficulty of comparing the times for both models, the temporal positions of the first luminosity maxima were chosen to be the same and a numerical time shift of the maxima thus cannot be revealed. The largest difference of the gravitational wave luminosity appears at the secondary maximum at $t \approx 4.6$ ms after

---

[1]　When the hydrodynamics code uses the relation of Eq. 2, heating means a change of the constant K in the polytropic equation of state, Eq. 1.

the actual merging event. In our simulations this maximum is a factor of 2.5 higher than that shown in Zhuge et al. (1994). In addition, our Model ZCM displays a tertiary maximum at $t \approx 7.3$ ms, with the time intervals between the maxima being roughly 2.5 ms. The much more prominent secondary and tertiary maxima in our Model ZCM are due to the fact that the rotating merged object has a strongly quadrupolar structure and performs oscillations and pulsations: two revolving "subcores" can be seen in Fig. 1 which continue to emit gravitational waves for as long as they are present and rotate.

The integrated energy emitted in gravitational waves is $2.0 \cdot 10^{52}$ erg which corresponds to 0.79% of Mc^2, M being the mass of one neutron star. If one extracts the analogous values for the gravitational wave energy from Fig. 16b in Zhuge et al. (1994) for the time interval shown in Fig. 3, one obtains 0.8% of Mc^2, in very good agreement with our Model ZCM, because the smaller peaks of the gravitational wave luminosity in the model of Zhuge et al. (1994) are compensated by their larger widths.

For completeness we also show in Fig. 4 the gravitational wave forms for Model ZCM, which can be compared with Fig. 15 of Zhuge et al. (1994). After the maximum amplitude is reached, the wave form of model ZCM is damped by roughly a factor of two within 10 further periods, while the damping factor is about 20 in the simulations of Zhuge et al. (1994). This difference reflects the motion of the two persisting "subcores" in our model.

3.4. Gravitational wave spectrum

The cumulative emission of gravitational wave energy as a function of frequency is shown in Fig. 5. In the upper part of each panel, the downward sloping straight line represents the energy loss per unit frequency interval of a point-mass binary. The frequencies to the left of the vertical line correspond to the wave frequencies that are emitted before the start of the numerical modelling, i.e. for times $t < 0$. We produce a combined wave by using the quadrupole moments for a point-mass binary for $t < 0$ and taking the numerically obtained quadrupole moments at $t > 0$ (in analogy to Zhuge et al. 1994). The combined wave is then Fourier analysed up to the times given in the lower left corners of the panels of Fig. 5.

At low frequencies the energy spectrum calculated for the combined wave fits very well to what is expected from the point-mass approximation. Although the merged object in the simulation radiates gravitational waves for a longer time than the point-masses, the very much smaller amplitudes associated with the coalescence of extended neutron stars result in less energy emitted at almost all higher frequencies. By Fourier transforming the signal of the combined wave until different times $t > 0$, we are able to roughly locate the moments when the peaks are produced.
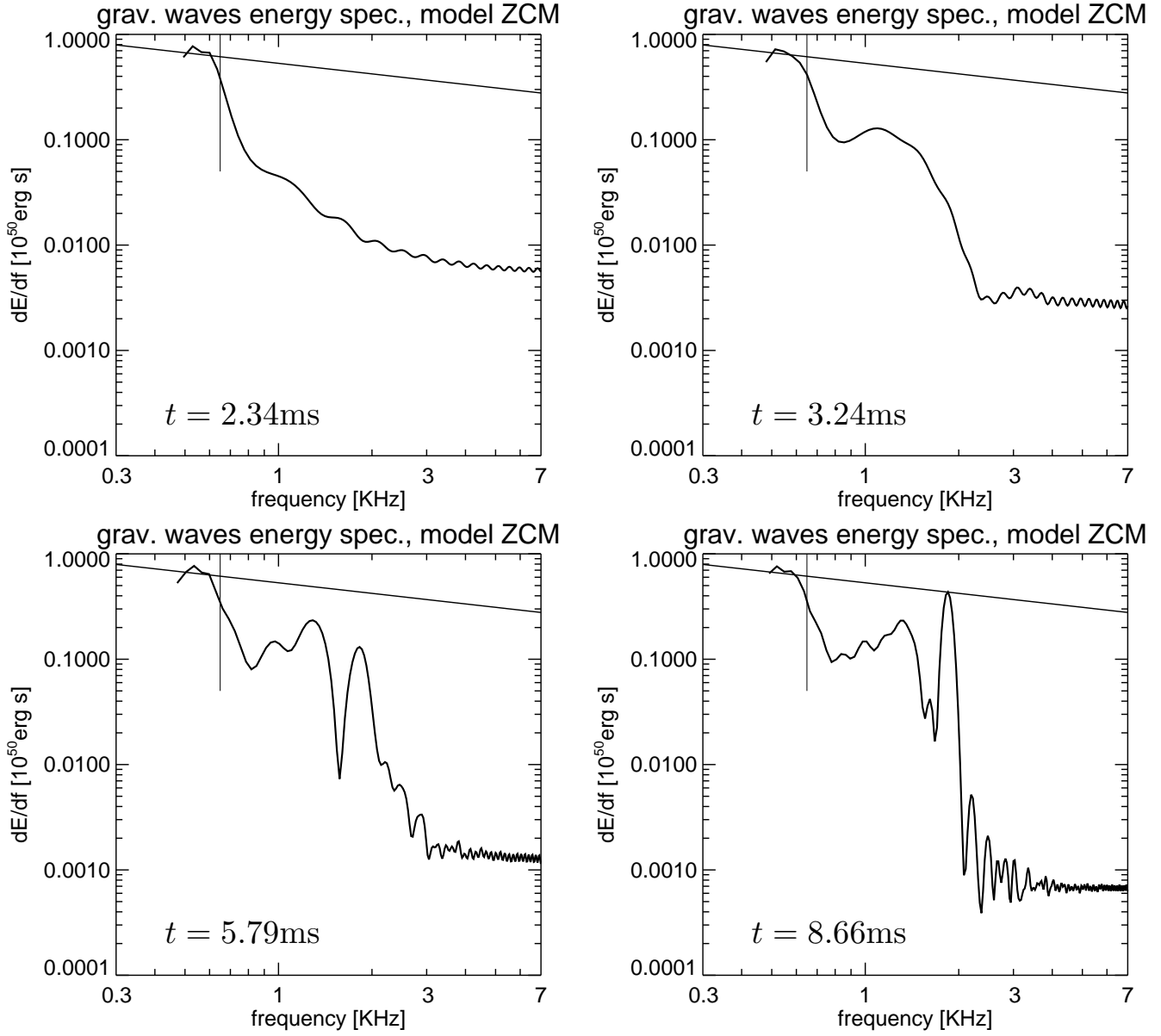
Fig. 5. Energy spectrum of gravitational waves emitted in Model ZCM. The times until which the Fourier transforms are performed are indicated in the lower left corner of the panels. They correspond to the snapshots of the density distributions shown in Fig. 1. The straight, downward sloping line is the spectrum of a point-mass binary. The vertical lines indicate the frequency corresponding to the orbital frequency of two point masses at the initial distance of the neutron stars in our numerical model

At around $t \approx 2.3$ ms the spectrum is structureless. A peak at roughly $f \approx 1.14$ KHz starts to form at $t \approx 3.24$ ms and has saturated by $t \approx 5.79$ ms and shifted to around $f \approx 1.22$ KHz. A second peak around $f \approx 1.67$ KHz is visible at this time but continues to grow until $t \approx 8.7$ ms and to shift to $f \approx 1.79$ KHz. The timing of the two peaks corresponds very well to the three maxima of the gravitational wave luminosity (Fig. 3): the peak at $f \approx 1.22$ KHz is formed by the first outburst of gravitational wave emission and the $f \approx 1.79$ KHz peak by the second and third phases of strong emission. Fig. 17 in Zhuge et al. (1994) displays the corresponding wave spectrum for their model. One notices that (a) we confirm their dip below 1 KHz, (b) we also see the slight rise above 1 KHz, (c) they quote a value for a peak at 1.75 KHz which we indeed find at 1.79 KHz, and (d) their 1.75 KHz peak is significantly smaller than the one of our model. Thus the overall shape of the spectrum of our Model ZCM is similar to the spectrum of Run 2 of Zhuge et al. (1994). The visible differences, in particular the high frequency spectrum and the spectral maximum at $f \approx 1.75$ KHz (point (d) above), are associated with the fact that due to

the quadrupolar deformation of the merged object in our simulation the emission of gravitational waves continues for a longer time than in Run 2 of Zhuge et al. (1994). This emission of waves at higher frequencies is an indication that the merged object becomes more compact with time. The gravitational waves emitted between 4 ms and 8 ms (Fig. 3) have a frequency of roughly 1.8 KHz, while those originating between 2 ms and 4 ms have around 1.2 KHz.

We can only speculate why our Model ZCM wobbles around and oscillates for a longer time than the merger in the simulation of Zhuge et al. (1994). To calculate their model they used only 1024 SPH particles, which is at least an order of magnitude less than the number of zones resolving the central part of the merged object in our Model ZCM. Thus it seems possible that in Zhuge et al. (1994) a larger numerical viscosity of the SPH code damps out the quadrupolar pulsations more quickly than in our calculations. Another possible cause for the different oscillation behaviour of our Model ZCM compared to Zhuge et al. (1994) might be the differences of the physical description, namely the lack of tidal deformations in the initial state and the implementation of backreaction terms in Model ZCM. The fact that Model ZCM does not initially have any tidal bulges and thus is not in equilibrium with the gravitational field will lead directly to oscillations of the neutron stars reflected e.g. in the values of the maximum density. This has been observed clearly in previous models, e.g. see Fig. 10 in Ruffert et al. (1996), in which one sees that the oscillations have a period of one dynamical time (i.e. the fundamental mode) and damp out in roughly 10 periods. Although the wobbling noticed in model ZCM might conceivably be triggered by this initial disequilibrium, the former is surely not sustained by the latter: the wobbles continue for a time over which the initial oscillations are damped out. The effect of the different implementation of the gravitational wave backreaction is more difficult to assess, but in general it has a damping effect. Initially, when the neutron stars are well separated, the backreaction terms are responsible for the decay of the orbit, i.e. the spiral-in of the neutron stars. This phase is simulated with similar effect by Model ZCM and Zhuge et al. (1994), since without gravitational waves the neutron stars would circle each other practically indefinitely. However, during the final plunge and the subsequent evolution Zhuge et al. (1994) do not include any backreaction. Once the neutron stars have come close enough, hydrodynamic effects alone dominate the merging process (cf. Rasio & Shapiro 1994 and references therein). Our Model ZCM is thus subjected to more damping during the final stages of the merging process than in Zhuge et al. (1994), so this again cannot explain the longer-term wobbling.

4. Results of Model SNO

4.1. Initial conditions

In Model SNO we use the same mass and radius for the neutron stars and the same adiabatic exponent ($\Gamma = 2$) as Shibata et al. (1992) for their Model III. Thus, we place the two neutron stars with a mass of $M = 1.4\ M_\odot$ each and a radius of 9 km at an initial distance of 27 km. The two main differences between our run and the one of Shibata et al. (1992) are (1) the hydrodynamical integrator, and (2) the initial rotational state of the neutron stars and the correspondingly constructed equilibrium configuration. Although the algorithm to calculate the gravitational wave backreaction terms is the same in both works, we integrate the hydrodynamic equations with the PPM scheme, in contrast to Shibata et al. (1992) who employed a finite difference method that is *not* based on a Riemann-solver. In a number of previous models Nakamura & Oohara (1991) considered neutron stars at rest in a corotating system which is equal to a solid-body type rotation in an inertial frame. Contrary to that, Model III of Shibata et al. (1992) was constructed as a "spinning" model, because the neutron stars were given spins in the corotating frame. Corresponding to this neutron star rotation Shibata et al. (1992) assumed axisymmetric neutron stars in rotational equilibrium initially, but did not solve for the equilibrium configuration in the common gravitational potential, arguing that tidal forces are much smaller than self-gravity. However, with the velocity distribution chosen by Shibata et al. (1992) the initial velocities of all parts of the neutron stars are collinear in an inertial frame, say parallel to the y-axis, and the neutron stars do not rotate. We therefore construct our neutron star models with the same velocity distrubution as unperturbed spherical polytropes, whereby we also assume that tidal forces are small compared to self-gravity. We consider it to be more plausible that, if no spin is present in the inertial system, spin rotational deformation does not need to be taken into account either.

In their publication Shibata et al. (1992) show the density distribution and flow pattern as functions of time for Model III as well as the gravitational wave forms and the gravitational wave luminosity. We shall therefore concentrate on these quantities in the comparison of Model III of Shibata et al. (1992) and our Model SNO.

4.2. Dynamical evolution

Snapshots of the density distribution in the orbital plane together with the velocity field are shown at six instants in Fig. 6. The panels could, in principle, be compared with the panels of Fig. 3 of Shibata et al. (1992), respectively. In practice, however, the direct comparison of these contour plots is difficult, unfortunately, since Shibata et al. (1992) do not use contour values that are constant in time and, moreover, they plot arrows to indicate the flow field, but do not specify the actual magnitude of the fluid
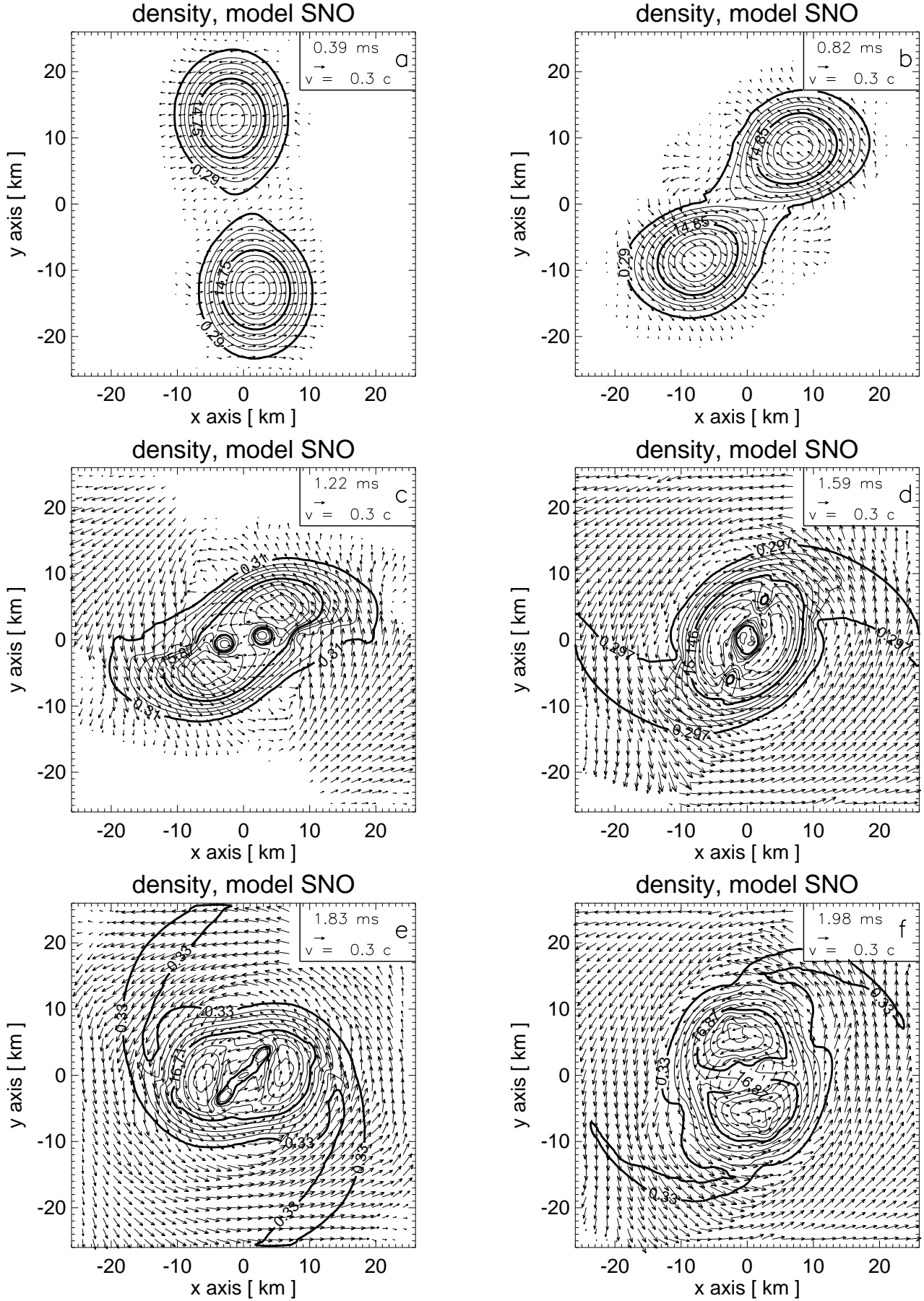
Fig. 6. Cuts in the orbital plane of Model SNO at six instants in time showing the density contours together with the velocity field. The density contours are linearly spaced in intervals of $0.1\rho_{max}$ starting at $0.01\rho_{max}$ and are labeled in units of 10^{14}g/cm^3. The legend at the top right corner of each panel gives the scale of the velocity vectors and the time elapsed since the beginning of the simulation
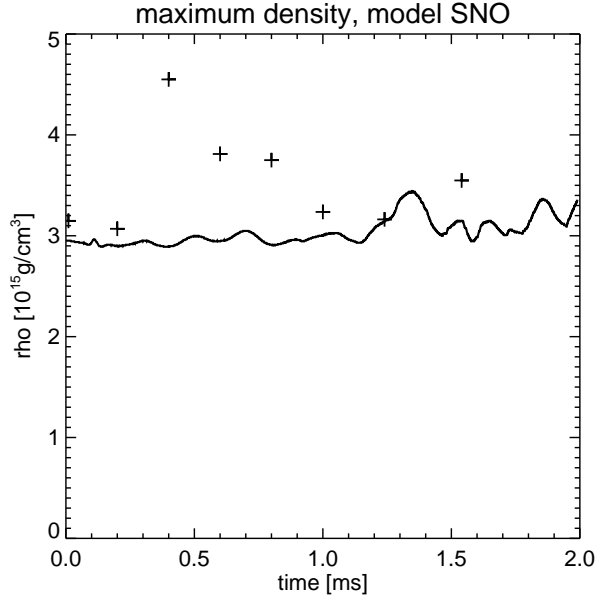
Fig. 7. The maximum density on the grid as a function of time for Model SNO (solid line). The maximum density values as deduced from Fig. 3 of Shibata et al. (1992) are indicated by crosses
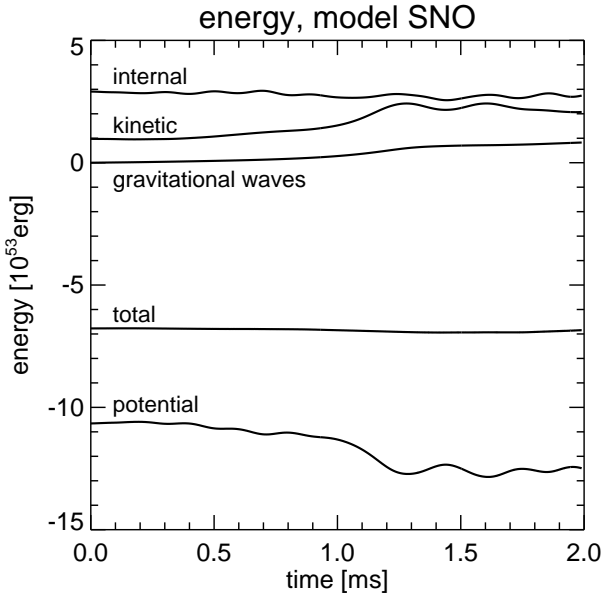

Fig. 8. Kinetic energy, internal energy, gravitational potential energy, and emitted gravitational wave energy as functions of time for Model SNO. The total energy contains all individual energies
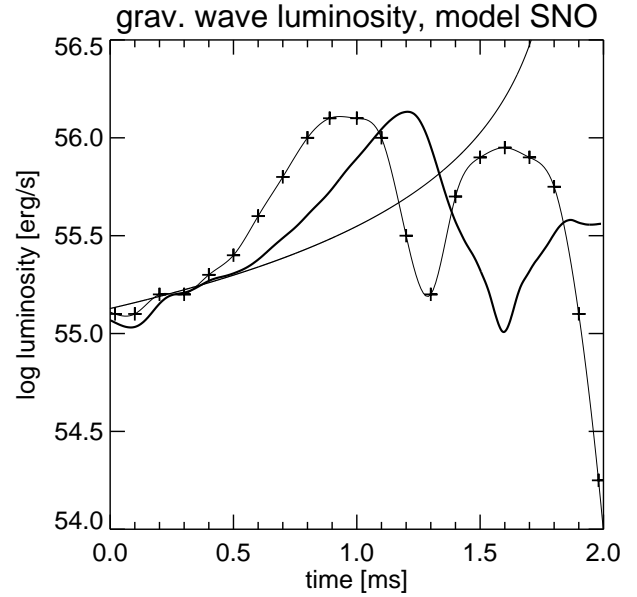

Fig. 9. The gravitational wave luminosity as a function of time for Model SNO (bold). The crosses represent the values taken from Fig. 6b of Shibata et al. (1992). They are connected by splines. The monotonically rising curve represents the luminosity of a point-mass binary

velocities. We used their prescription for the values of the density contours in Fig. 6.

One can recognize that initially, at $t \approx 0.4$ ms and at $t \approx 0.8$ ms, our Model SNO is still in agreement with the one of Shibata et al. (1992). However, at $t \approx 1.2$ ms two distinct minima appear between the cores of the neutron stars in Model SNO, while in Model III of Shibata et al. (1992) the most prominent minimum is at the center in between the neutron stars. These two minima of our Model SNO merge to form the central minimum at $t \approx 1.6$ ms, while two secondary minima are additionally present to the sides of the central minimum. Thus Model SNO at $t \approx 1.6$ ms resembles Model III, albeit at a different time, $t \approx 1.2$ ms. This indicates a shift in time by roughly $\Delta t \approx 0.3$ ms of the temporal evolution of both models that will become more clear in the next section. The three minima between the neutron star cores merge again, forming one elongated string by $t \approx 1.8$ ms. The structure of the merged object with two sub-cores remains present until the end of our simulations at $t \approx 2$ ms, while the density valley between becomes less prominent.

A quantity better suited for comparison is the maximum density as a function of time, the values of which can be found inserted in the panels of Fig. 3 of Shibata et al. (1992). In Fig. 7 these values are displayed at eight points in time, together with the maximum density for our Model SNO. The maximum density of Model III by Shibata et al. (1992) peaks at around $t \approx 0.4$ ms which is different from our Model SNO. It is hard to explain
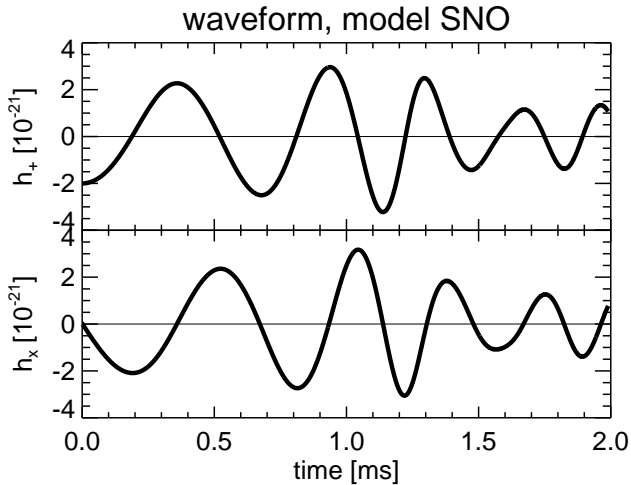
Fig. 10. The gravitational wave forms, h_+ and $h_\times$, for Model SNO as observed on the z-axis at 10 Mpc distance

this difference of the density evolution without having more detailed information about Model III of Shibata et al. (1992). At the time the density maximum occurs in the latter model, the neutron stars are still clearly separated, in both their Model III (Fig. 3c in Shibata et al. 1992) and in our Model SNO (Fig. 7). There is an indication that at $t \approx 0.4$ ms the density distribution in the neutron stars of Shibata et al. (1992) develops a "crack" or "discontinuity". The "crack" seems to emanate from the center and propagate along the direction of the x- and y-axes in both neutron stars. We speculate that this might cause the higher density maximum at $t = 0.4$ ms in the model of Shibata et al. (1992). The reason for the differences in the evolution of the maximum density and the neutron star separation seems not to be associated with the initial shape and structure of the neutron stars due to the different assumptions about the neutron star spins. Rather than differences of the mass distributions, the different momenta of the stars might be responsible for the discrepant evolution.

In Fig. 8 we show the temporal evolution of some integral energy quantities: the potential, kinetic, internal energies as well as the energy in gravitational waves and the total sum of all energies. The total energy is conserved to 1% compared to the maximum potential energy. The more compact structure of the merged object is reflected in the deeper potential at the end of the simulation. Note the slight oscillation present especially in the potential and kinetic energies which shows the wobbling of the subcores. The internal energy hardly changes indicating that the merging process proceeds rather softly without strong shocks.

4.3. Gravitational wave forms and luminosity

Figure 9 displays the gravitational wave luminosities as functions of time for Model SNO and for Model III of Shibata et al. (1992; Fig. 6b). The maximum of the emission (which is located in the model of Shibata et al. (1992) at $t \approx 0.9$ ms) is shifted in time by $\Delta t \approx 0.3$ ms, but agrees in height to within 10%. Note that model SNO follows the point-mass binary approximation for roughly 0.2 ms longer than Model III. We assume that (a) this initial deviation of Model III is primarily responsible for the subsequent time shift visible in the density contours and the gravitational wave luminosity, and that (b) the initial deviation is due to the differing initial rotational states of the neutron stars. Since the separation at the beginning of the simulations is very close to the dynamic stability limit (cf. Lai et al., 1994, and references cited therein) a small difference in density distribution can cause a substantial time lag: if the neutron stars are initially further separated than the stability limit, gravitational wave emission has to continue for some time to drive the decay of the orbit before the dynamical instability can set in.

For completeness we also show in Fig. 10 the gravitational wave forms for Model SNO which can be compared with Fig. 6a of Shibata et al. (1992). Due to the time shift mentioned above, the signal of our Model SNO is roughly one wave period shorter at the end of the simulation than Model III.

5. Results of Model RJS

5.1. Initial conditions

Model RJS is calculated with neutron stars which have the same mass, radius, and central density as those in Model A64 of Ruffert et al. (1996). Using the Lane-Emden equation and the mass–radius relation, this was achieved by appropriately adjusting the polytropic constant K and the adiabatic exponent Γ (cf. Table 1) for the equation of state. Placing the neutron stars at the same initial distance of 42 km and giving them the same velocity distribution as in as Model A64, we are left with a model differing only in the employed equation of state: Model RJS uses a polytopic equation of state according to Eq. 2, while Model A64 was calculated with the equation of state of Lattimer & Swesty (1991) and included the effects due to neutrino emission.

Out of the variety of quantities shown and discussed in Ruffert et al. (1996), we decided to compare the evolution of the mass distribution, the separation of the density maxima as a function of time to show possible differences in the dynamics, and the luminosity, wave form, and energy spectrum of the gravitational wave emission.
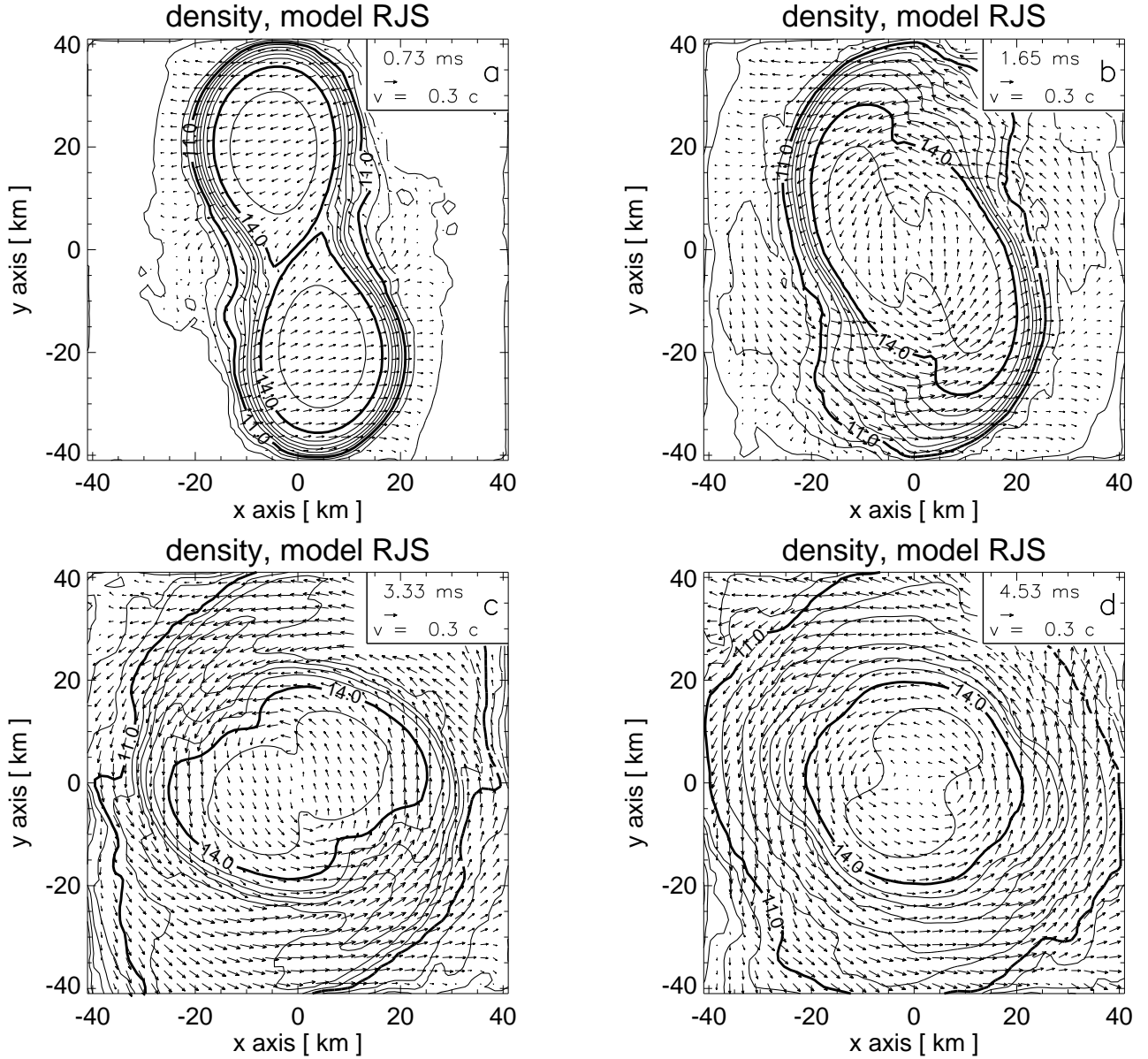
Fig. 11. Cuts in the orbital plane of Model RJS at four instants in time showing the density contours together with the velocity field. The density contours are logarithmically spaced with intervals of 0.5 dex. The density is measured in units of g/cm^3. The bold contours are labeled with their respective values. The legend at the top right corner of each panel gives the scale of the velocity vectors and the time elapsed since the beginning of the simulation

5.2. Dynamical evolution

The contour plots in Fig. 11 show the dynamical evolution. The mass distribution is visualized by density contours with arrows superimposed to indicate the flow velocities. These plots can directly be compared with the Figs. 4c, 4e, 5a, and 5c of Ruffert et al. (1996), respectively. Initially, until about $t \approx 1.7$ ms, only minor differences occur. At $t \approx 1.7$ ms the neutron star surfaces towards the downstream sides (at the positions $x \approx 0$ km, $y \approx \pm 20$ km) are more extended in Model RJS (Fig. 11b) than in Model A64 of Ruffert et al. (1996) (see Fig. 4e there). This effect also can be seen in Fig. 11c where the

contour for the density value of 10^{11} g/cm^3 extends further out than the marginal "spiral arm" visible in Fig. 5a in Ruffert et al. (1996).

Compared to the models computed with the equation of state of Lattimer & Swesty (1991) in Ruffert et al. (1996), all three models discussed here, ZCM, SNO, and RJS, have a less steep density decline at the neutron star surface and develop a more extended disk after merging. This general phenomenon is explained by the stiffness of the polytropic equations of state which have adiabatic exponents between 2 and 2.32. This is much stiffer than the equation of state of Lattimer & Swesty (1991) in the
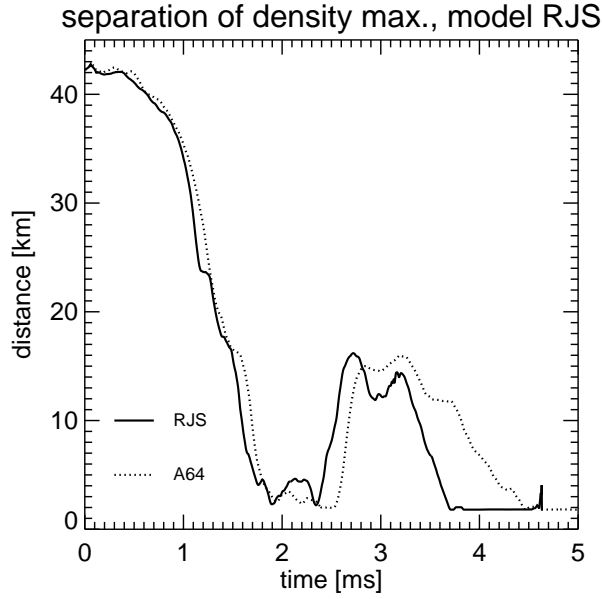
Fig. 12. The separation of the density maxima of the two neutron stars as a function of time for Model RJS (bold) and for Model A64 (dotted) of Ruffert et al. (1996)
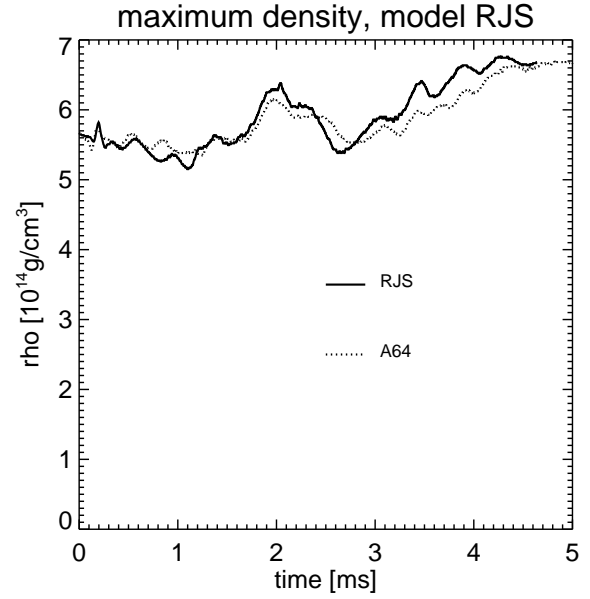
Fig. 13. The maximum density on the grid as a function of time for Model RJS (bold) and for Model A64 (dotted) of Ruffert et al. (1996)

subnuclear regime, where $\Gamma \approx 1.33$ to 1.66. An increase of the internal energy, e.g. by the dissipation of kinetic energy in shocks or via shear effects, which is important in the regions close to the surface, therefore, leads to a strong pressure increase and thus to an inflation of the stellar layers involved.

In the core region of the merged object, Figs. 11c and 11d reveal more fine structure than Model A64 of Ruffert et al. (1996; Fig. 5a and 5c) which indicates a stronger damping of high-frequency oscillation modes in the latter model, caused by the bulk viscosity of the physical equation of state used there. At time $t \approx 4.5$ ms both simulations show a rather similar overall structure of the merger (compare Fig. 11d to Fig. 5c in Ruffert et al. 1996). In both cases the innermost density contour ($\rho \approx 3 \cdot 10^{14}$ g/cm^3) is dumb-bell shaped and the underlying double-core structure means that the merging process is still going on. Also during this phase the exterior layers at subnuclear densities are significantly more extended in Model RJS due to the stiffer polytropic equation of state.

On the whole, the coalescence in Model RJS proceeds very similarly to Model A64 of Ruffert et al. (1996). Figs. 12 and 13 show the separation of the density maxima and the value of the maximum density as functions of time for the two models. In both models the neutron star density maxima merge within 2 ms and then separate again for a short while when the double-core structure forms (between 2.5 ms and about 3.5 to 4 ms) because of the large angular momentum of the merged object. Model RJS comes to "rest" faster (by roughly 0.5 ms) than Model A64 which has separated density maxima

from 2.5 ms to 4.5 ms. This difference might be caused by a larger angular momentum transport outwards through the more extended disk of Model RJS. This hypothesis is strongly supported by the outwardly directed velocity field which can be seen in Fig. 11d, indicating mass and angular momentum loss accross the grid boundaries. Notice also that due to the differences of the subnuclear equation of state the transition from the central core of the merged object to the disk region is less sharp in Model RJS (compare Fig. 11b with Fig. 5c in Ruffert et al. 1996).

Before the neutron stars merge, their central density decreases slightly by about 5% (see Fig. 13) and during the coalescence the maximum density increases by about 20% of the initial value. The overall dynamical behaviour, reflected by the separation of the density maxima and the value of the maximum density, reveals much less difference between the models than can be seen from the density contours. The similar dynamics can easily be understood because the construction of the initial neutron stars and the adjustment of the parameters K and Γ in the polytropic equation of state Eq. 1 should ensure very similar behaviour (e.g response to compression) of the polytropic equation of state and the Lattimer & Swesty (1991) equation of state in the nuclear and supranuclear regimes. The differences occur in the outer regions of the neutron stars at densities below the nuclear matter density where the polytropic equation of state for the chosen value of Γ is much stiffer than the equation of state of Lattimer & Swesty (1991). This difference mainly concerns the evolution of the outer layers and thus the formation, structure and properties of the disk that forms during merging.
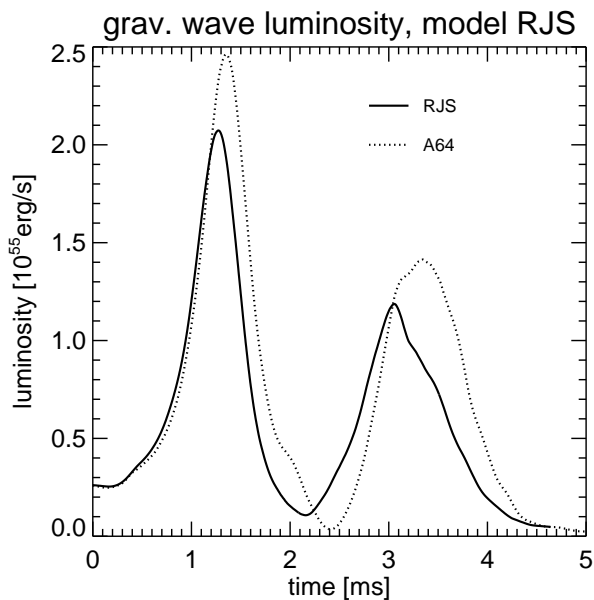
Fig. 14. The gravitational wave luminosity as a function of time for Model RJS (bold) and Model A64 (dotted) of Ruffert et al. (1996)

Fig. 15. The gravitational wave forms, h_+ and $h_\times$, for Model RJS (bold) and Model A64 (dotted) of Ruffert et al. (1996)

Since, however, only a comparatively small fraction of the neutron star mass has densities less than nuclear matter density, the overall dynamical evolution of the bulk of the matter is unaffected by the difference of the low-density equation of state. From the gradual increase of the density maximum we conclude that the merging is as smooth as in Model ZCM and not so violent as in Model SNO where the density increases rapidly during the final coalescence (see Fig. 7).

5.3. Gravitational wave forms and luminosity

The gravitational wave luminosity is a very sensitive indicator of differences in the overall dynamical evolution and the mass distributions, since it involves the third time derivative of the quadrupole moment. One recognizes from Fig. 14 that the main maximum of the gravitational wave luminosity is lower by 20% and slightly narrower in Model RJS compared to Model A64. Roughly the same statements apply to the second maximum. These differences between the two models are concordant with the temporal behaviour of the separation of the density maxima in both models (see Fig. 12), but are much smaller than the differences between Models A64, B64, and C64 of Ruffert et al. (1996).

The wave forms (Fig. 15) show only minor differences: both the amplitudes and the phases of the signals coincide well. Slight discrepancies develop after $t \approx 2$ ms which corresponds to the time after the first merging of the density maxima has occurred (Fig. 12) and the gravitational wave emission reaches a maximum (Fig. 14). Once the separate
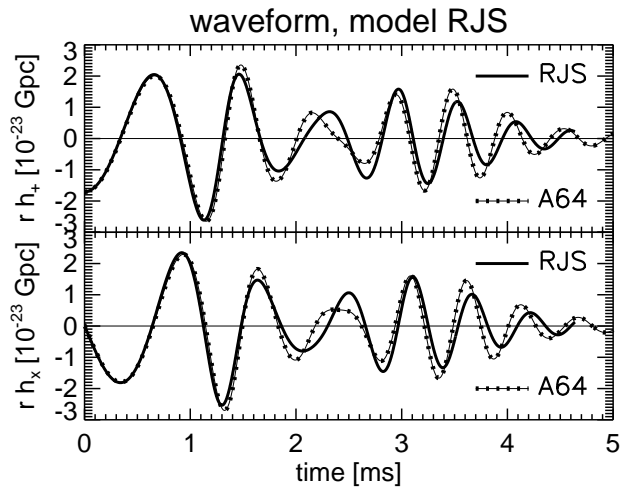
density maxima have vanished, the merged configuration has loses its strongly quadrupolar deformation and therefore radiates gravitational waves less efficiently.

In agreement with the temporal displacement of the evolution visible in Figs. 12, 13, and 14, a small phase shift of the gravitational wave forms after $t \approx 2$ ms is caused by the slightly faster rotation of Model A64. The higher angular momentum of the merged configuration (see above) together with the more compact structure of the layers at intermediate densities (between 10^{12} g/cm^3 and 10^{14} g/cm^3) due to the less stiff equation of state, is also the reason for somewhat larger gravitational wave amplitudes and the enhanced gravitational wave luminosity in case of Model A64 at times later than about $t \approx 3$ ms. The total energy emitted in gravitational waves in Model RJS is $2.8 \cdot 10^{52}$ erg, roughly 20% less than the $3.4 \cdot 10^{52}$ erg emitted by Model A64 within 5 ms (taken from Fig. 23 of Ruffert et al. 1996).

5.4. Gravitational wave spectrum

The close resemblance of the gravitational wave forms (Fig. 15) is mirrored in the gravitational wave spectra which share the main features in the two models RJS and A64 from Ruffert et al. (1996). The spectra of Model RJS can be found in Fig. 16 and should be compared with Fig. 28 in Ruffert et al. (1996). They contain the same kind of information as already described in the context of Fig. 5, i.e. the frequency distribution of the gravitational wave energy emitted until the times shown in the lower left corners of the plots, together with a line representing the energy loss per unit frequency interval of a point-mass binary.

At time $t \approx 3.2$ ms the spectra look very similar and Models RJS and A64 both have a spectral minimum at $f \approx 1$ KHz and spectral maxima at $f \approx 1.3$ KHz and $f \approx 2.0$ KHz. Even for frequencies $f > 2.0$ KHz the decline of the spectra is pretty much the same. The major visible differences are the strengths of the second and of the third spectral maximum at $f \approx 2.4$ KHz. While the maximum at $f \approx 2$ KHz is more pronounced in Model RJS, the peak at $f \approx 2.4$ KHz is higher than in Model A64. In both models the $f \approx 1.3$ KHz maximum is mainly generated before $t \approx 3.2$ ms, while the $f \approx 2$ KHz maximum grows strongly after $t \approx 3.2$ ms. The $f \approx 2$ KHz maximum tends to shift to $f \approx 1.8$ KHz (more clearly in Model RJS) between $t \approx 3.2$ ms and $t \approx 4.64$ ms and becomes slightly more prominent in Model RJS than in Model A64. After $t \approx 4.6$ ms the spectral peaks at frequencies between about 2 KHz and 2.4 KHz have merged into one structure in Model A64, while in Model RJS there are still two sharp, well separated maxima and the $f \approx 2.4$ KHz feature has not gained much strength any more. We think that these results can again be explained by the stronger pulsational and vibrational activity of Model A64 after merging which adds to the power of the gravitational wave emission at frequencies around and above $f \gtrsim 2$ KHz.

6. Discussion and summary

The hydrodynamic simulations presented in this work follow the dynamical evolution and the gravitational wave emission of two merging neutron stars modeled as polytropes. We compared our results with three models published earlier and tried to obtain information about uncertainties and differences caused by the numerical scheme employed for integrating the hydrodynamic equations, by the numerical resolution and setup of the initial model, and by the use of a polytropic equation of state instead of the physical equation of state of Lattimer & Swesty (1991). We chose the following three models for comparison: (a) "Run 2" of Zhuge et al. (1994), (b) "Model III" of Shibata et al. (1992), and (c) "Model A64" of Ruffert et al. (1996). We attempted to construct the initial configurations as similar to these models as possible and also used polytropic equations of state which were the same or which guaranteed to reproduce the properties (mass, central density, radius) of the neutron stars.

6.1. Model ZCM

Run 2 of Zhuge et al. (1994) is different from our Model ZCM in (a) one numerical aspect: Zhuge et al. (1994) used an SPH algorithm while we employed the grid-based PPM scheme and (b) two physical aspects: (i) the gravitational wave backreaction is prescribed in an *ad hoc* way by Zhuge et al. (1994), because it is included in the computation when the neutron stars are still separate but switched off during the merging process; (ii) both computations start with different initial separations and tidal deformations. Our Model ZCM seems to retain a "double core" structure and thus a large quadrupolar deformation during the merging for a longer time than Run 2. This has two consequences: On the one hand, the secondary and tertiary maxima of the gravitational wave luminosity are significantly higher in our calculation, and on the other hand, the peak in the gravitational wave spectrum at a frequency of $f \approx 1.8$ KHz is more prominent, too (a first maximum is present at about 1.3 KHz). Both effects are caused by a more extended post-coalescence period in Model ZCM where the merger performs "ringing" and "wobbling" motions and emits more power in gravitational waves at frequencies around $f \approx 1.8$ KHz. We find a local minimum of the gravitational wave spectrum at a frequency of about $f \approx 1.5$ KHz in good agreement with Run 2 of Zhuge et al. (1994), although this minimum is not quite as deep in our calculation. The integrated gravitational wave energy in both models is also nearly the same, implying that the stronger emission of our Model ZCM at high frequencies is accompanied by a deficit at lower frequencies, which we indeed find in the band $f \approx 0.7$–1.1 KHz. We suppose that these differences are mainly caused by the larger numerical viscosity of the SPH code and the comparatively poor resolution with only 1024 particles in the computation of Zhuge et al. (1994). Although the two main physical differences (initial tidal deformations, backreaction implementation) could in principle be also partly responsible for the wobbling, we assume their effect to be small: (i) the initial disequilibrium due to tidal deformations has been shown (Ruffert et al. 1996) to be damped out within a time shorter than the ringing, and (ii) the gravitational backreaction has a damping effect in the longer-term merging process.

6.2. Model SNO

Shibata et al. (1992) performed their calculations with a finite difference grid-based explicit Eulerian code just as we do, albeit with a different hydrodynamical integrator, a second order advection using a method proposed by LeBlanc (see Appendix A of Oohara & Nakamura 1989), which does not make use of a Riemann solver. They incorporated the gravitational wave backreaction in a way conceptually equivalent to our treatment. Their grid had 121^3 zones. To solve the Poisson equation, the Incomplete Cholesky decomposition and Conjugate Gradient (ICCG) method by Meijerink & van der Vorst (1977) was used. Contrary to this we implemented a fast Fourier method and our grids had a size of 128×128 (and 32 zones vertical to the orbital plane). However, long before any hydrodynamical interaction between the neutron stars occur, at $t \approx 0.4$ ms when the neutron stars just barely touch each other, the maximum density on the grid showed an extreme value in the calculations of Shibata et al. (1992) which we were unable to reproduce in our Model SNO.
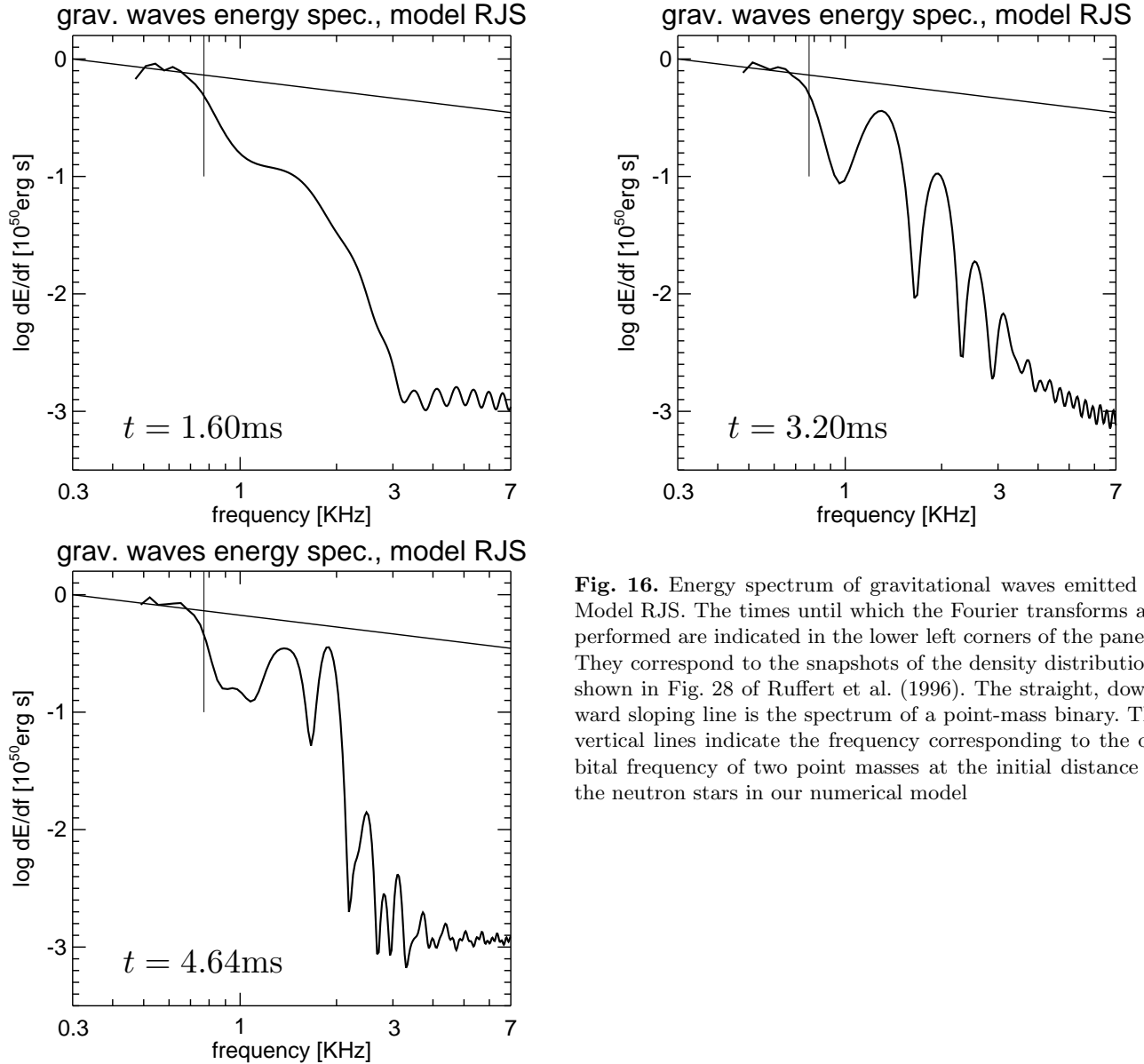
grav. waves energy spec., model RJS

$t = 1.60$ms

grav. waves energy spec., model RJS

$t = 3.20$ms

grav. waves energy spec., model RJS

$t = 4.64$ms

Fig. 16. Energy spectrum of gravitational waves emitted in Model RJS. The times until which the Fourier transforms are performed are indicated in the lower left corners of the panels. They correspond to the snapshots of the density distributions shown in Fig. 28 of Ruffert et al. (1996). The straight, downward sloping line is the spectrum of a point-mass binary. The vertical lines indicate the frequency corresponding to the orbital frequency of two point masses at the initial distance of the neutron stars in our numerical model

This difference is difficult to explain and we can only speculate that it might be associated with the choice of Shibata et al. (1992) to use configurations in rotational equilibrium for the two neutron stars which were given spins in the frame that corotates with their orbital revolution. Because these spins of the stars were absent for an observer in an inertial frame and because Shibata et al. (1992) did not construct equilibrium configurations in the common gravitational field of the two stars (which would make more sense), we did not follow their choice but started our simulations as usual with spherical neutron star models. This obvious discrepancy causes an initial delay of the merging by $\Delta t \approx 0.3$ ms in our model SNO compared to Model III of Shibata et al. (1992). Nevertheless, the gravitational wave luminosity amplitude of their model and of our simulation coincide surprisingly well to within 10%.

6.3. Model RJS

In a third comparative study we performed a simulation, Model RJS, with initial conditions (neutron star masses, radii, central densities, initial separation, and velocities) like those used in Model A64 of Ruffert et al. (1996). The only major difference was that instead of the physcial equation of state of Lattimer & Swesty (1991) — which also allowed us to include neutrino physics in the computation — we used a polytropic equation of state in Model RJS with the initial value of the parameter K and the constant adiabatic index Γ adjusted such that the initial neutron star properties are reproduced.

We found the overall dynamical evolution during the coalescence, e.g. timescale of merging, formation of spiral-arm-like structures of matter spun off the neutron star

surfaces by tidal and centrifugal forces, post-merging oscillations and pulsations, to be very similar in both models. This is particularly clearly seen in the behaviour of the neutron star separation and of the maximum density on the grid as functions of time. Correspondingly, the gravitational wave luminosity, gravitational wave form, and gravitational wave spectrum share the main structural features. The peak gravitational wave luminosity and the total energy emitted in gravitational waves are only about 20% smaller in the polytropic model. The gravitational wave forms are very similar but have the tendency to develop a slight phase shift after the two neutron stars have merged into one object. These minor differences reflect the fact that the properties of the Lattimer & Swesty (1991) equation of state in the nuclear and supranuclear regimes — which are most important for the neutron star structure as well as for the gravitational wave signature during the merger — are sufficiently well reproduced. This is ensured by our determination of the equation of state parameters K and Γ by prescribing the same mass, central density and radii of the neutron star models constructed with the polytropic equation of state and with the Lattimer & Swesty (1991) equation of state.

The minor differences of both calculations, the roughly 20% smaller peak emission of gravitational waves in the polytropic case and the small phase shift of the gravitational wave forms, are mainly caused by differences of the equations of state in the subnuclear regime ($\rho \lesssim 10^{14}$ g/cm^3). In this regime in particular, the description of the properties of neutron star matter with an equation of state with a uniformly chosen adiabatic exponent Γ is inadequate. With the employed value of $\Gamma = 2.319$ the equation of state at subnuclear densities is by far too stiff. As a result, the neutron star surface layers in Model RJS were more extended and the density decline less sharp compared to Model A64 in Ruffert et al. (1996). Morerover, during merging the neutron star surfaces came into contact earlier in Model RJS which moderated the dynamical interaction of the stars and reduced the luminosity outburst of gravitational waves during this phase. After merging, the overestimated stiffness of the equation of state led to a slightly less compact central body of the merger in Model RJS and to a significantly more extended disk structure surrounding the central, massive body than in Model A64. In particular, the properties of this disk, its mass, radial extent, and rotational state, therefore require the use of a proper physical equation of state during the simulations of neutron star merging.

References

Abramovici A., et al., 1992, Science 256, 325

Blanchet L., Damour T., Schäfer G., 1990, MNRAS 242, 289

Bradaschia C., et al., 1991, in *Gravitation*, Proc. Banff Summer Inst., Banff, Alberta; eds. R. Mann & P. Wesson; World Scientific, Singapore

Colella P., Woodward P.R., 1984, JCP 54, 174

Danzmann K., et al., 1995a, *GEO 600 – A 600 m Laser Interferometric Gravitational Wave Antenna*, Proc. of the first Edoardo Amaldi Conference, Frascati, June 1994, to be published by World Scientific (Singapore)

Danzmann K., et al., 1995b, *LISA – Laser Interferometer Space Antenna for gravitational wave experiments*, Proc. of the seventh Marcel Grossmann Meeting, Stanford, July 1994, to be published by World Scientific (Singapore)

Davies M., Benz W., Piran T., Thielemann F.K., 1994, ApJ 431, 742

Dermer C.D., Weiler T.J., 1995, astro-ph/9508047

Eastwood J.W., Brownrigg D.R.K., 1979, JCP 32, 24

Finn L.S., Chernoff D., 1993, Phys.Rev.D 47, 2198.

Finn L.S., 1994, in *Proc. of the Lanczos International Centenary Conference*, eds. D. Brown et al. SIAM, Philadelphia

Lai D., Rasio F.A., Shapiro S.L., 1994, ApJ 420, 811

Lattimer J.M., Swesty F.D., 1991, Nucl. Phys. A535, 331

Meijerink J.A., van der Vorst H.A., 1977, Math. Comp. 31, 148

Nakamura T., Oohara K., 1991, Prog. Theor. Phys. 86, 73

Oohara K., Nakamura T., 1989, Prog. Theor. Phys. 82, 535

Oohara K., Nakamura T., 1990, Prog. Theor. Phys. 83, 906

Press W.H., Flannery B.P., Teukolsky S.A., Vetterling W.T., 1992, *Numerical Recepies*, Cambridge Univ. Press

Rasio F.A., Shapiro S.L., 1994, ApJ 432, 242

Reisenegger A., Goldreich P., ApJ 426, 688

Ruffert M., Janka H.-Th., Schäfer G., 1996, A&A 311, 532

Shibata M., Nakamura T., Oohara K., 1992, Prog. Theor. Phys. 88, 1079

Shibata M., Nakamura T., Oohara K., 1993, Prog. Theor. Phys. 89, 809

Thorne K., 1992, in *Recent Advances in General Relativity*, eds. A. Janis & J. Porter, Birkhäuser, Boston

Zhuge X., Centrella J.M., McMillan L.W., 1994, Phys.Rev.D 50, 6247